Extension of PS-InSAR Approach for DEM and Linear Deformation Rates Estimation. Case Study of Bucharest Area

Cosmin Dănișor, University Politehnica of Bucharest, cosmin.danisor@yahoo.com, Romania
Mihai Datcu, German Aerospace Center, Mihai.datcu@dlr.de, Germany

Abstract

Persistent Scatterers interferometry represented a breakthrough in synthetic aperture radar processing, its initial approach covering the linear deformation rates estimation step. Most advanced differential interferometric methods prefer the use of an external digital elevation model, because of the difficulties of unwrapping an interferometric phase which contains also the topographic component. In this work, the persistent scatterers approach is extended also for digital elevation model estimation, by applying the minimum cost flow phase unwrapping algorithm solely on the detected PS network. A detailed presentation of the proposed processing chain is conducted, along with the results of the described algorithm's implementation on a test region from Bucharest city, using a dataset of 12 Sentinel-1 acquisitions.

1 Introduction

Synthetic Aperture Radars (SAR) [1] are very popular systems in the remote sensing field, the continuous development of the related processing techniques being also helped by the improvement of the resolution capabilities of recently launched sensors. Their advantages, which allow the acquisition of images independently of sunlight and weather conditions are already well documented [1].

SAR interferometry (InSAR) [2] is based on coherent processing of 2 acquisitions, being used mostly for topography measurements. Differential interferometry (D-InSAR) [2] subtracts the topographic component from the interferometric phase, in order to estimate scene's displacements. Advanced D-InSAR techniques [3]-[6] exploit the baseline and temporal diversity of a multiple acquisitions dataset, having the proven capability to estimate the linear deformation rates of the terrain with millimetre accuracy.

Multiple directions have been approached in case of multi-baseline/multi-temporal techniques. Persistent Scatterers Interferometry (PS-InSAR) [3] identifies the points showing high temporal correlation. Further interferometric processing steps are implemented exclusively in the selected points, because residual interferometric phase estimation is expected to be more precise in case of PS, so the processing can lead to very precise results. In addition, construction of interferograms solely on the detected points also lowers the constraints imposed on dataset's baseline values. In order to limit the effects of decorrelation, small baselines subset algorithm (SBAS) [4] analyses solely the multi-look differential interferograms generated from image pairs with small perpendicular and temporal baselines. Those pairs are obtained by an appropriate combination of dataset's images.

Coherent point targets analysis (CPT) [5] is a two-steps method which combines both PS-InSAR and SBAS approaches. The former method is employed for coarse-scale processing, to estimate the digital elevation model (DEM) errors and atmospheric artefacts. This first step is complemented by the later approach, which is used to estimate the deformation rates in the stable targets of the scene. To avoid the employment of two processing algorithms, SqueeSAR method [6] makes use of the statistical proprieties of both permanent and distributed scatterers, to develop a common processing technique applicable for both scenarios.

This paper is structured as following: section 2 discusses the proposed extension (also at the DEM generation step) of the PS-InSAR approach, while in section 3 the detailed processing chains for images pre-processing, DEM estimation and phase regression analysis are presented along with the obtained results. Conclusions and further directions are addressed in the final section.

2 Proposed Extension of PS-InSAR Algorithm

To generate the differential interferograms, topographic component Φ_{topo} must be estimated and subtracted from the interferometric phase Φ_{itf} (Φ_{fl} is the earh's curvature component, Φ_{ldef} is the linear deformation rates contribution and Φ_{res} the residual component):

$$\Phi_{itf} = \Phi_{topo} + \Phi_{fl} + \Phi_{ldef} + \Phi_{res} \quad (1)$$

ISBN 978-3-8007-4636-1 / ISSN 2197-4403

To achieve this, most works presented in literature [3]-[6] suggest the use of an external DEM, the most popular choice being the SRTM. However, resolution of those external DEMs is much lower compared to the resolution capabilities of current SAR sensors, and a conversion step of the DEM from ground to radar geometry is required. The most delicate part of the interferometric processing is the phase unwrapping, this being the main reason why the DEM computation is in general avoided. To lower phase variations, most of the advanced D-InSAR methods firstly subtract the topographic component estimated from the external DEM in order to facilitate the unwrapping process. In the original PS-InSAR approach [3], DEM generation/import step is conducted before the selection of PS candidates, the PS processing being employed exclusively for differential interferometric steps (which include the refinement of DEM values).

Recently launched SAR missions present a reduced revisit time, especially in case of tandem satellites. This advantage might be exploited by selecting an image pair with low temporal and high perpendicular baselines to estimate the scene's DEM. Temporal decorrelation is reduced, but atmospheric propagation effects are still a potential source of error. The proposed processing chain for linear rates deformation is presented in **Figure 1**. Its steps will be detailed in Section 3.

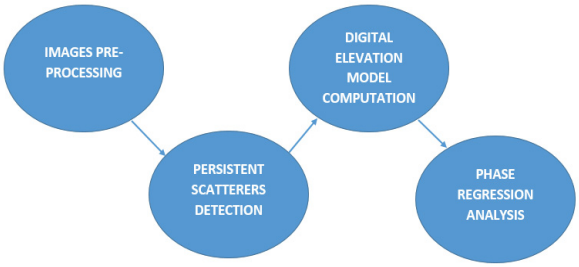

Figure 1: General steps of the employed processing chain

Main difference compared to the original PS-InSAR method consists in the fact that PS approach is extended also for the DEM estimation process, as the selected candidates will be used during the most critical step of DEM generation – phase unwrapping. One of the most popular phase unwrapping algorithms is the minimum cost flow (MCF) method [7]. To avoid noise propagation, MCF algorithm is initially implemented only on highly coherent regions of the interferogram – a validity mask is defined to exclude the areas with high phase noise. This mask can be generated during the foregoing step of the unwrapping – phase filtering, by designing an adaptive filter based on the local fringe spectrum. The gaps imposed by the validity mask into the initial unwrapped result are then filled by interpolation.

In the proposed chain, by conducting the stable targets detection before DEM generation, the derived PS map will be used as validity mask for the unwrapping process. Therefore, the MCF algorithm is carried exclusively in the points needed for further processing during the phase regression analysis stage, so no interpolation step is required in this case. Since those points are detected considering the low decorrelation criterion, the results of the unwrapping process are expected to be reliable. Analysis of phase regression contains anyway a step which takes into account possible DEM-related errors and corrects them. In conclusion, the DEM is expected to be accurately generated in points needed for the differential processing. Another advantage of the proposed technique consists in the fact that the DEM is directly generated in SAR system's acquisition geometry, thus avoiding a supplementary conversion and coregistration steps. Furthermore, its resolution is equal to the one of dataset's SAR images.

3 Implementation of the Proposed Algorithm. Results

3.1 Dataset

The proposed processing chain is applied to estimate the linear deformation rates from Politehnica University – Crângași – Primăverii area of Bucharest city, Romania, using a stack of Sentinel-1 acquisitions. The algorithm is implemented using the interferometric SAR processing (ISP) and interferometric point targets analysis (IPTA) packages [8]-[9] of Gamma software. The dataset consists of 12 SLC images acquired by Sentinel-1 constellation in TOPS mode, having a range resolution of 5 m and azimuth resolution of 20 m. The images were acquired between April and June 2017, having a temporal baseline range of 66 days. Mater image of the dataset was selected to have its acquisition moment situated near the central point of dataset's temporal range. Dataset's perpendicular baselines range is equal to 160.5 m.

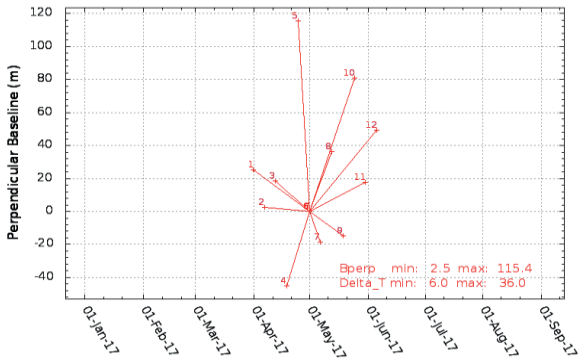

Figure 2: Perpendicular and temporal baselines of dataset's acquisitions

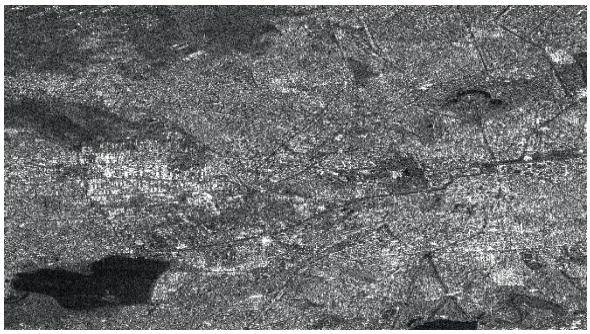

Figure 3: Amplitude of test region from dataset's master image. Acquisition date: 01.05.2017

Spatio-temporal baseline's distribution is presented in **Figure 2**. Amplitude of test region is presented in **Figure 3**. This area is also situated near Morii lake, which in clearly distinguishable in the previous figure.

3.2 Images Pre-processing

Coregistration of dataset's images needs to be done at sub-pixel accuracy, especially in azimuth direction, otherwise Doppler frequency shifts between consecutive bursts, specific to TOPS acquisition mode, will affect the further interferometric processing. This operation was implemented in 3 steps – a coarse coregistration and two refinement iterations. Even if the test region was contained in a single burst, 3 bursts were selected in this step, because bursts overlap regions are essential for this stage.

Coarse coregistration consists in images alignment based on orbital information. Since orbit parameters of Sentinel-1 images are accurate, this step represents a reliable starting point, which estimates constant offset values in range and azimuth. First refinement step calculates intensities cross-correlation R in various paths w defined across the scene (I_m and I_l represent master and slave images intensities):

$$R = \frac{\sum_{l \in w} I_m(l) I_s^*(l)}{\sqrt{\sum_{l \in w} |I_m(l)|^2 \sum_{l \in w} |I_s(l)|^2}} \quad (2)$$

Variable offsets are estimated in both direction in the form of high-order offset polynomials, which are used to resample the slave acquisitions into master image geometry. Final refinement step is a spectral diversity method, which computes the double phase difference in the bursts' overlap regions. This difference varies proportionally with the coregistration error, therefore it's possible to convert it to azimuth offset correction. This step is vital to avoid the occurrence of interferometric phase jumps between consecutive bursts during further processing steps.

Coregistration step was validated by generating the coarse interferograms of the three-burst image portion. No phase jumps were observable at the delimitation regions.

3.3 Persistent Scatterers Detection

Two methods were employed for PS identification. First method studies the temporal statistics of target's amplitude, while the second method considers scatterer's spectral proprieties. Both algorithms are broadly presented in [10]. Firstly, all burst SLCs are deramped using the phase ramp of the master image. Temporal variation is quantified by amplitude's mean-per-sigma ratio *MSR* computation in each resolution cell of the scene. This ratio is expected to present a value above unit in case of stable targets (μ represents the amplitude mean and σ its standard deviation):

$$MSR = \frac{\mu}{\sigma} \quad (3)$$

Second method classifies as PS points which present low variation of spectral phase. To estimate this parameter, power spectral density $q_g(\omega)$ is analysed, being computed according to Wiener-Hincin theorem, as the Fourier transform of data's autocorrelation R_g

$$q_g(\omega) = \sum_k R_g(k) e^{-j\omega k} \quad (4)$$

Furthermore, a point is classified as PS only if its amplitude value is greater than the mean amplitude of neighbouring pixels, this constraint being imposed to avoid the PS detection in regions affected by shadowing phenomenon. For further processing, the test region was separated along the coregistered dataset.

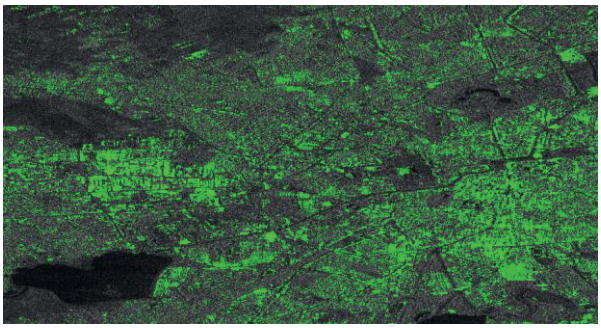

Figure 4: Spatial distribution of the identified PS

Figure 4 presents the spatial distribution of PS detected in the test region. A number of 193623 stable targets were identified, which represents 11.52% of scene's resolution cells.

3.4 Digital Elevation Model Estimation

The revisit time of Sentinel-1 constellation is equal to 6 days. The interferometric pair used for DEM generation was selected to have to have minimum temporal base-

line (25.04 – 01.05.2017 acquisition dates) and high perpendicular baseline, 115.4 m, to increase the sensitivity of interferometric topographic component Φ_{topo} to terrain's height h (b_p is the perpendicular baseline of the pair, λ radar's wavelength, R the sensor-scene distance and θ is the incidence angle):

$$\phi_{topo} = \frac{4\pi}{\lambda} \frac{h \cdot b_p}{R \cdot sin\theta} \quad (5)$$

The main steps of the interferometric processing chain employed for DEM computation are presented in **Figure 5**:

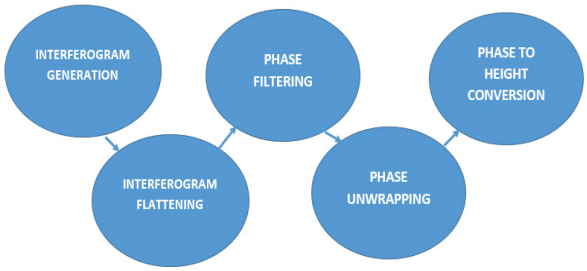

Figure 5: Steps of DEM computation, which can be carried exclusively on the detected PS network

Since the coregistration was implemented at dataset level, it is no longer required at this step. Because of Doppler centroid variations not properly represented in image parameter files and small baseline values, common band filtering is not applied. The contribution of earth's curvature is estimated and removed from the interferometric phase using the orbital and baseline parameters of the images pair. Adaptive phase filtering is employed, since this step is an essential precursor of the unwrapping process. The adaptive filter is designed based on the local fringe spectrum, its transfer function H being non-linearly dependent on interferometric power spectrum I:

$$H = I^{a} \quad (6)$$

where coefficient α belongs to $[0,1]$ domain.

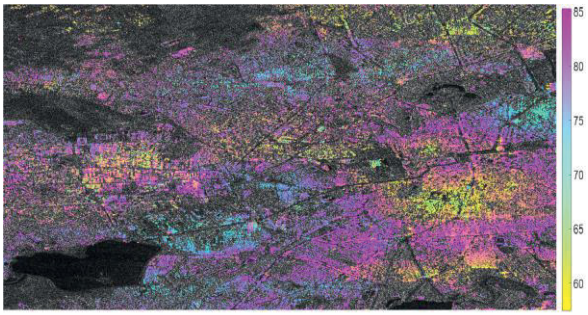

Figure 6: Estimated DEM heights

Phase unwrapping is conducted by implementation of the proven MCF method [7] on the network of detected PS. Since this network represents the validity mask of the proposed chain, no amplitude or phase noise coherence estimation is required, and, as previously mentioned, no interpolation of MCF solution is needed.

The values of the unwrapped phase are then converted to terrain heights, considering also the interferometric pair's perpendicular baseline value. The estimated DEM heights of the test area are presented in **Figure 6**.

3.5 Phase Regression Analysis

Initial differential interferograms are generated in the PS points by subtracting the estimated topographic component from the flattened interferometric phase. For pairs with low perpendicular baseline, the differential interferograms do not present high spatial variations, as the one presented in **Figure 7**.

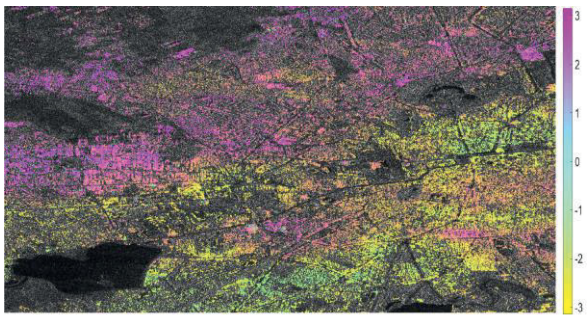

Figure 7: Differential phase; image pair with 17.74 m perpendicular baseline (01.05 – 31.05.2017)

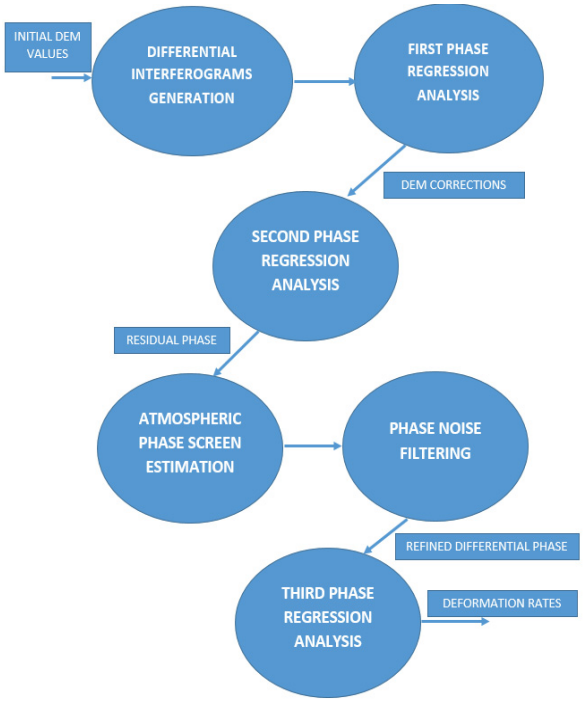

Figure 8: Representation of phase regression analysis iterations

Unwrapping of the differential interferograms is carried before further processing. The employed regression model takes into account the linear variation of the subtracted topographic component with the perpendicular baselines and the proportional variation of linear deformation rates with the temporal baselines. Therefore 2D phase regression analysis iterations in aspect to perpendicular and temporal baselines will be employed. The phase regression is not expected to perfectly match the employed 2D model, since DEM errors and residual interferometric components are present. Therefore, a best fit solution is searched. The linear deformation rates estimation process includes three iteration of regression analysis, its block diagram being presented in **Figure 8**:

First regression analysis iteration returns an initial estimation of linear deformation rates, DEM-related errors, the residual interferometric component and a quality measure for each PS, given by its standard deviation from the regression model. A number of 48403 low quality points will be eliminated from further analysis, which represents 24.99% of initial PS candidates. Eventual unwrapping related errors are also identified and corrected during this step. Second regression iteration uses the DEM corrected values and first deformation rates approximations to re-estimate the residual interferometric phase Φ_{res}, which is then interpreted to separate its 3 main components: atmospheric phase screen Φ_{atm}, noise Φ_n and non-linear deformation rates Φ_{ndef}:

$$\Phi_{res} = \Phi_{atm} + \Phi_n + \Phi_{ndef} \tag{7}$$

Atmospheric phase screen is estimated as the large scale component of the residual phase, by means of spatial filtering. An exemplification of estimated atmospheric phase screen is presented in **Figure 9**:

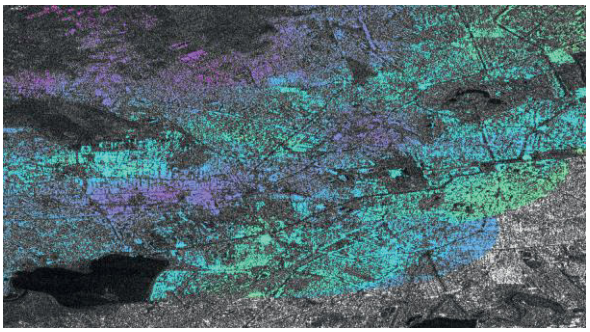

Figure 9: Estimated atmospheric phase screen, 31.05.2017 acquisition

The atmospheric component is subtracted, and the phase noise is reduced also by means of filtering. Having reduced the residual component, a third regression analysis is computed for a final estimation of linear deformation rates.

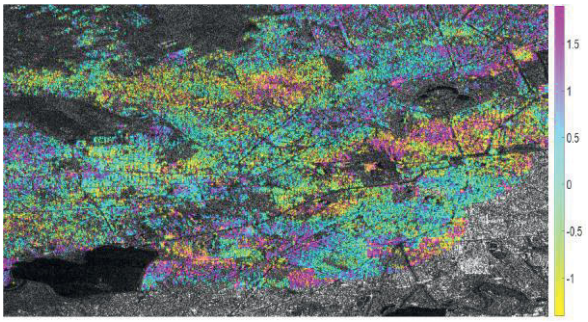

Figure 10: Linear deformation rates (cm/year) estimated with the extended PS-InSAR approach

The final output of the presented processing chain, consisting of the estimated linear deformation rates in the test region, is presented in **Figure 10**.

4 Conclusions

Main contribution of this paper consists in extension of PS-InSAR approach also for the scene's DEM estimation process. A detailed description of the employed processing chain is presented, along with the results of the algorithm's implementation on a 12 images Sentinel-1 dataset of Bucharest city.

Validation of estimated DEM heights was conducted by comparison of the values range with the one of external SRTM-90 model.

Linear deformation rates derived by implementation of the proposed extension of PS-InSAR on the Bucharest test area vary between -1.4 and 1.9 cm/year, which represents a realistic range. Validation of those results can only be conducted by comparison with other studies of subsidence phenomenon, implemented in the same area. No such experiments carried in exactly the same period (April – June 2017) have yet been published, but similar studies have been conducted in the past in Bucharest city [11],[12], using images acquired by different sensors, including ERS. Range of linear deformation rates estimated in those works is similar to the one obtained by our proposed approach.

As future work, the obtained linear deformation rates will be compared with the ones that will be obtained in an ongoing bi-static experiment currently carried in the test area. A tomographic approach [13] using a dataset with larger orbital tube can also be employed for scene's elevation values estimation.

ISBN 978-3-8007-4636-1 / ISSN 2197-4403

Acknowledgements

Authors wish to thank Antonio Pepe and Gianfranco Fornaro from CNR-IREA, Italy for their suggestions regarding the paper framing. This work has been conducted within the frame of research project *SPERO – Space technologies used in the management of disasters and major crises, manifested at local, national and regional levels*, funded from the Minister of Research and Innovation, UEFISCDI, project reference: PN-III-P2-2.1-SOL-2016-03-0046

References

[1] Bamler, R. "Principles of synthetic aperture radar." *Surveys in Geophysics* 21.2 (2000): 147-157.

[1] Bamler, R and Hartl, P. "Synthetic aperture radar interferometry" *Inverse problems* 14.4, (1998)

[2] Ferretti, A., Prati, C., & Rocca, F. "Permanent scatterers in SAR interferometry". *IEEE Transactions on geoscience and remote sensing*, *39*(1), (2001): 8-20

[4] Berardino, P., Fornaro, G., Lanari, R., & Sansosti, E. "A new algorithm for surface deformation monitoring based on small baseline differential SAR interferograms" *IEEE Transactions on Geoscience and Remote Sensing*, *40*(11) (2002): 2375-2383.

[5] Lanari, R., Mora, O., Manunta, M., Mallorquí, J. J., Berardino, P., & Sansosti, E.. "A small-baseline approach for investigating deformations on full-resolution differential SAR interferograms" *IEEE Transactions on Geoscience and Remote Sensing*, *42*(7) (2004): 1377-1386.

[6] Ferretti, A., Fumagalli, A., Novali, F., Prati, C., Rocca, F., & Rucci, A. "A new algorithm for processing interferometric data-stacks: SqueeSAR". *IEEE Transactions on Geoscience and Remote Sensing*, *49*(9) (2011): 3460-3470

[7] Pepe, A., & Lanari, R. On the extension of the minimum cost flow algorithm for phase unwrapping of multitemporal differential SAR interferograms. *IEEE Transactions on Geoscience and remote sensing*, *44*(9), (2006): 2374-2383.

[8] *** - Gamma Interferometric SAR Processor, ISP User's Guide, (2014)

[9] *** - Gamma Interferometric Point Targets Analysis Software, IPTA User's Guide, (2014)

[10] Dănişor, C., Popescu, A., & Datcu, M.: "Persistent scatterers detection on synthetic aperture radar images acquired by Sentinel-1 satellite". *Advanced Topics in Optoelectronics, Microelectronics, and Nanotechnologies VIII* (2016)

[11] Armaş, I., Mendes, D. A., Popa, R. G., Gheorghe, M., & Popovici, D. Long-term ground deformation patterns of Bucharest using multitemporal InSAR and multivariate dynamic analyses: a possible transpressional system?. *Scientific Reports*, *7*, 43762. (2017).

[12] Armaş, I., Necsoiu, M., Mendes, D. A., Gheorghe, M., & Gheorghe, D. Ground Displacement Trends in an Urban Environment Using Multi-Temporal InSAR Analysis and Two Decades of Multi-Sensor Satellite-Based SAR Imagery. In *9th International Workshop Fringe*. (2015)

[13] Fornaro, G., Serafino F. & Soldovieri. F. "Three-dimensional focusing with multipass SAR data." *IEEE Transactions on Geoscience and Remote Sensing* 41.3 (2003): 507-517